

Order and disorder, crossovers, and phase transitions in dipolar artificial spin ice on the Cairo lattice

Yuriy Shevchenko ^{*}, Vladislav Strongin , Vitalii Kapitan , Konstantin Soldatov , Aleksandr Makarov , Mihail Padalko, Roman Volotovskii , and Konstantin Nefedev [†]

Institute of High Technologies and Advanced Materials, Far Eastern Federal University, Vladivostok, Russky Island, Ajax 10, 690922, Russian Federation
and Institute of Applied Mathematics, Far Eastern Branch, Russian Academy of Science, Vladivostok, Radio 7, 690041, Russian Federation

 (Received 15 December 2021; revised 1 November 2022; accepted 8 November 2022; published 5 December 2022)

We study the thermodynamic properties of the magnetic dipolar spin ice on a 2D pentagonal Cairo lattice by using the numerical Metropolis and the complete enumeration methods. We use the model of point Ising-like dipoles considering long-range interactions with up to 100 nearest neighbors and with periodic boundary conditions. There are two explicit peaks both in the temperature behavior of the heat capacity and in the magnetic susceptibility. The low-temperature peak is caused only by long-range interactions and is not present in the model where each dipole interacts only with four nearest neighbors. The height of the peak depends logarithmically on the quantity of dipoles, which indicates a phase transition. The nature of the low-temperature phase transition is related to the transformation from order to disorder in orthogonal sublattices while maintaining the spin ice state and the spin ice rule in the sublattice of crosses. The high-temperature heat capacity peak is associated with the melting of spin ice, i.e., with the crossover from spin ice to paramagnetic chaos. Its height is constant and does not depend on the quantity of dipoles. It is shown that the choice of the radius of the dipole-dipole interaction has a significant effect on the statistical properties of the model. The model may even show the appearance of the long-range order and the phase transition in the case of long-range interaction or its absence in the case of short-range interaction.

DOI: [10.1103/PhysRevE.106.064105](https://doi.org/10.1103/PhysRevE.106.064105)

I. INTRODUCTION

Artificial spin ice is a group of metamaterials consisting of magnetic nanoscale islands arranged so that the resulting structure exhibits collective magnetic properties that a single particle does not have.

The island in frames of the dipole model can be represented as a single-domain nanodimensional ferromagnetic capable of interacting with other islands through dipole-dipole exchange. It is oval-shaped, which leads to magnetic anisotropy along the long axis, making its behavior Ising-like. The volume is chosen so as to be a single domain, and at the same time, the magnetic field induced by neighboring islands was enough to change the magnetic moment of an island. Due to these properties, the island mimics the behavior of a point Ising-like dipole.

The lattice geometry may impose configuration constraints, due to which not all pairwise interactions can be simultaneously satisfied. This phenomenon is called frustration, and systems are frustrated. The first experimentally created structure was the square spin ice, aimed at mimicking the magnetic behavior of the atomic lattice of the pyrochlores $\text{Dy}_2\text{Ti}_2\text{O}_7$ and $\text{Ho}_2\text{Ti}_2\text{O}_7$ [1] in planar projection [2–4]. It is much easier to experimentally observe nanoscale islands on

a plane than atoms in a bulk. A fine tuning of the lattice geometry of the artificial spin ice and the shape of the islet becomes possible. This allows us to choose convenient values of physical parameters, such as magnetic susceptibility, anisotropy, energy barriers between similar energy configurations, etc. Thus, new geometries of 2D spin ices have been proposed that have no analogs among existing materials.

A distinct class is vertex-frustrated lattices [5,6], where it is impossible to choose all vertices to be in their lowest energy configuration, due to topological constraints. As a result, these vertex-frustrated structures always contain excited vertices. These include derivatives of spin ice structures like Brickwork [7,8], Shakti [4,9,10], Tetris [11], Santa Fe [12], and Saint George [13] and others like kagome [4,14–18] and Cairo [19–23] [Fig. 1(a)].

Some computational studies on spin ice consider interactions only between the nearest neighbors [10,14–16,24], treating the long-range energy as zero in order to simplify the calculations, which is not always justified, or represent vertex interactions as “dumbbells” or “charge” models, which are also short range. The dipole-dipole interaction depends on distance r between dipoles and in some cases can cause long-range ordering [4,25]. This has been shown for the 3D tetrahedral lattice of pyrochlore [26,27], where the number of neighbors changes as $\sim r^3$ and the dipole energy of one pair as $\sim r^{-3}$. So the total energy induced by far-distant neighbors is of the same order and can compete with the energy of the

^{*}shevchenko.yuriy.a@gmail.com

[†]nefedev.kv@dvfu.ru

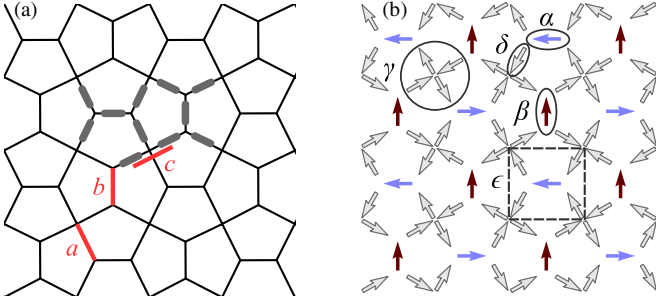


FIG. 1. 2D Dipolar spin ice on a Cairo lattice. (a) Ferromagnetic islands are shown as gray ovals. Letters a , b , c denote lattice parameters. (b) One of the possible GS configurations of Cairo dipolar spin ice with periodic boundary conditions both in short- and long-range interaction models. The point dipoles are in the middle of the arrows; the direction represents the magnetic moment. The key structural elements of the lattice are horizontal α , vertical β spins, and crosses γ consisting of δ spins. The unit cell of the lattice ϵ is shown as a square. The blue (silver) arrows are the moments directed along the field induced by its four nearest neighbors. The red (dim gray) arrows are the moments for which the magnetic field induced by the nearest neighbors is compensated.

nearest neighbors. The number of neighbors in a 2D lattice increases much slower, as $\sim r^2$.

In this paper we consider the dipolar spin ice on a 2D pentagonal Cairo lattice [19–23] [Fig. 1(a)], which is geometrically frustrated and seems to be a good candidate to research the effect of long-range interactions on the plane. Dipolar ferromagnetic islands are placed onto the bonds (edges) of the lattice. The longer side and the anisotropy axis of the island are aligned along the edge of the lattice. Previously it was shown that the point dipole model describes well the behavior of thermally active artificial nanosystems made of permalloy islands, e.g., kagome [28], square [29], and Cairo [23] spin ices. Each ferromagnetic island is associated with a point moment in the dipole model we use. The moments are located in the center of the nanoparticle and have a dipole-dipole interaction between themselves. As shown in [2], the oval shape of the nanomagnetic island induces a strong shape anisotropy, forcing it to be always magnetized along its long side. The shape anisotropy of the island is sufficient to use the Ising-like model; i.e., each magnetic moment has two states. The magnetic moment is located in the center of the island and is aligned with the corresponding edge of the lattice. Hereafter we will use the terms “spin” and “dipole,” which are synonymous with the “moment.”

The dipoles are marked with arrows in Fig. 1(b); the direction represents the direction of magnetization. The lattice structure consists of “crosses,” which like in square spin ice obey the ice rule “2-in and 2-out” in the ordered state. The crosses, together with additional spins, form pentagonal cells that produce closed chains and induce competing interactions.

We use the Monte Carlo simulation and the complete enumeration over all possible configurations in order to get and explain the temperature behavior of dipole spin ice on the Cairo lattice. In this paper we show that both the boundary conditions and the radius of the dipole-dipole interaction have a significant effect on the statistical properties of the model.

For example, the model may even show the appearance of a long-range order and phase transition (in the long-range interaction case) or its absence (in the short-range interaction case). The fine tuning of the volume of the nano-island and lattice parameters provides the ability to vary the temperature of the superparamagnetic transition. As a result, experimental observation of long-range order or disorder in the ground state (GS) in two-dimensional artificial spin ice becomes fundamentally possible [30].

II. THE DIPOLAR MODEL

We consider the two-dimensional pentagonal lattice discussed in [23]. Dipoles on the lattice form elementary cells ϵ containing five spins Fig. 1(b), translated in a checkerboard pattern so that neighboring cells are rotated relative to each other by 90° . There are $N = L \times L \times 5$ spins in the lattice, where L is the number of elementary cells along one side.

We conditionally divide the lattice into a sublattice of horizontally directed α , vertically directed β spins, which are located in the center of ϵ . δ spins form crosses γ [Fig. 1(b)].

The lattice is composed of irregular pentagons [Fig. 1(a)], where four edges have length a and one vertically or horizontally directed edge b . Parameter c defines the distance between the colinear dipoles δ , or in other words, determines the position of the spin δ on the edge of the lattice. An increase in c leads to a decrease in the energy of pair interactions inside γ and increases the energy of pair interactions in ϵ . By analogy with the experimental data [23], the lattice parameters are $a = 472$ nm, $b = 344$ nm, and $c = 376$ nm.

The interaction energy between dipoles i and j is defined as

$$E_{ij,\text{dip}}/D = s_i s_j \left(\frac{(\vec{m}_i \vec{m}_j)}{|\vec{r}_{ij}|^3} - 3 \frac{(\vec{m}_i \vec{r}_{ij})(\vec{m}_j \vec{r}_{ij})}{|\vec{r}_{ij}|^5} \right), \quad (1)$$

where \vec{m}_i is the moment of spin with unit length. The moment has only two possible opposite directions determined by Ising variables $s_i = \pm 1$. \vec{r} is the dimensionless radius vector normalized so that $|\vec{r}| = 1$ between points a apart. $D = \mu_0 \mu^2 a^{-3}$ is the dimensional coefficient required to relate the model of point dipoles to the macrospin model, μ_0 is vacuum permeability, μ is saturation magnetization of the nanoisland, and a is the lattice parameter described above. In this paper we consider a system with specific parameters, implying the volume of one island $300 \times 100 \times 2.6$ nm³ by analogy with [23]. The typical value of M_s for bulk permalloy is 8×10^5 A/m, but it is considerably lower for thin macrospins [28]. Here we use $M_s = 10^5$ A/m and $\mu = 7.8 \times 10^{-18}$ Am² $\approx 8.41 \times 10^5 \mu_B$, so $D = 7.27065 \times 10^{-22}$ J.

In the long-range interaction model, we do not take into account the energy of pairwise interactions, where $a|\vec{r}_{ij}| > 2000$ nm. Hereafter we will call this model “long-range.” We also consider the “short-range” case where interactions with $a|\vec{r}_{ij}| > 400$ nm are not taken into account. This distance is chosen so that each spin of the lattice has exactly four neighbors. In the short-range model, all four diagonally oriented spins of ϵ [Fig. 1(b)] will be neighbors for spins of type α and β . For spins of type δ , its neighbors are three adjacent spins in its cross and the nearest spin α or β .

We added a small vertical magnetic field $\vec{H} = \{0, H_y\}$, where $H_y = 1.5 \times 10^{-7}$, to the sample in order to calculate the magnetic susceptibility:

$$E = D \sum_{(i,j)} E_{ij,\text{dip}} - \mu_0 \mu M_s \sum_i s_i (\vec{m}_i \vec{H}), \quad (2)$$

where the summation $\langle i, j \rangle$ goes over all pairs of dipoles, within given interaction radius. The H_y value is dimensionless like $\vec{m}_{y,i}$. The dimensional constant $\mu_0 \mu M_s$ is in the same units as D .

Periodic boundary conditions (PBCs) are applied on all edges both to the short-range and to the long-range models. This allows us to get rid of the boundary effect and analyze low-energy configurations.

We use the canonical single-spin Metropolis algorithm to calculate thermodynamic averages [31,32]. Despite its simplicity, this still remains a popular method of statistical research in unexpectedly diverse sciences. The problem of obtaining a rigorous solution subexponentially fast for a large number of spins in the system is vital for a huge class of tasks. For numerical calculations at each specific temperature, we use 10^5 steps to prethermalize the system and 10^6 steps to calculate averages. This ensures that equilibrium is met. One step implies N Monte Carlo tries to flip a random s_i . We use a complete enumeration of all configurations to calculate the temperature behavior of entropy and analyze the GS.

Nonequilibrium thermodynamic effects, such as the coercive force of the island, are not considered in this paper, implying that all relaxation nonequilibrium processes have already been completed by the time of numerical experiments. The equilibrium for numerical Monte Carlo experiments is satisfied by preliminary Monte Carlo annealing. As for the exhaustive enumeration, the calculation of the complete group of events automatically means the fulfillment of the ergodicity condition.

III. THERMODYNAMICS OF CAIRO LATTICE

By means of the complete enumeration method and hybrid Monte Carlo method, it was shown in [33] that in the model of unrestricted interaction radius with the free boundary conditions for a finite relatively small quantity of dipoles on the Cairo lattice ($N = 20, 40,$ and 80) the degeneracy of the GS is not macroscopic. In the present work we performed an analysis of correlations, thermodynamic functions such as entropy, heat capacity, and magnetic susceptibility by means of Monte Carlo for $N = 5120$, and exactly calculated the GS for the Cairo lattice for long- and short-range interactions with PBCs in the case of $N = 20$.

A. Heat capacity, entropy, and effect of quantity of dipoles

Figure 2 shows the heat capacity comparing long-range ($a|\vec{r}_{ij}| < 2000$ nm) and short-range ($a|\vec{r}_{ij}| < 400$ nm) interaction models with $N = 5120$ dipoles obtained with the Monte Carlo method. We calculate it as

$$C(T) = \frac{\langle E^2 \rangle - \langle E \rangle^2}{k_B T^2 N}. \quad (3)$$

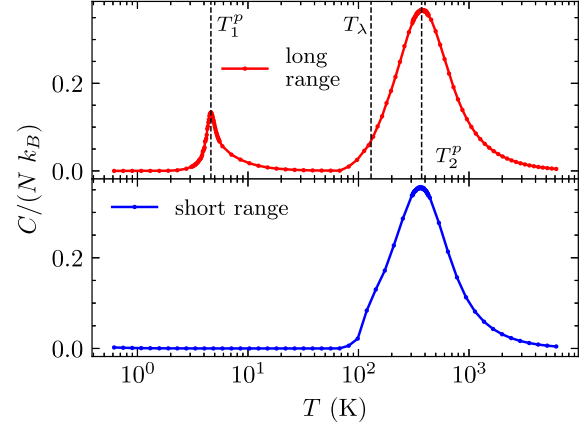


FIG. 2. Temperature dependence of the heat capacity $C(T)$ of the dipolar Cairo spin ice with $N = 5120$ dipoles and $c = 376$ nm in long-range (upper) and short-range (lower) models with PBCs. The dashed lines indicate the peaks of the heat capacity at $T_1^p \approx 4.62$ K, $T_2^p \approx 372.79$ K, and the critical temperature $T_\lambda \approx 130.00$ K.

The brackets $\langle \rangle$ denote Gibbs thermodynamic averaging at a specific T . The heat capacity has two pronounced peaks in the long range. At the same time, there is no low-temperature heat capacity peak for the short range. This means that the peak is caused only by long-range interactions. The dashed lines indicate the peaks of the heat capacity at $T_1^p \approx 4.62$ K and $T_2^p \approx 372.79$ K. In addition, we define the critical temperature $T_\lambda \approx 130.00$ K, which does not appear on the heat capacity curve. It will be described further. We also highlight these temperatures in Figs. 6–9 below.

It is currently unfeasible to consider all of 2^N configurations of the system when N is more than a few dozen due to exponential growth. The Monte Carlo algorithm we use is based on a partial sampling of the space of configurations with energies corresponding to the Gibbs distribution. The fraction of partial sampling and the sampling method itself often raises many questions about the convergence and reliability of the results. In addition, the Monte Carlo method does not allow the accurate calculation of entropy, because the degeneracy level (number of configurations) for a given energy is not available during partial sampling over the Gibbs distribution.

For a detailed explanation of the low-temperature behavior of the heat capacity, we obtained the exact solution of the entropy S as a function of temperature with the complete enumeration method for the studied models with $N = 20$. S is defined as

$$S = \frac{\langle E \rangle}{T} + k_B \ln \left[\sum_i g(E_i) \exp \left(\frac{-E_i}{k_B T} \right) \right], \quad (4)$$

where the summation goes over all possible values of energy of system and $g(E_i)$ is the quantity of configurations with E_i so that

$$\sum_i g(E_i) = 2^N. \quad (5)$$

We present the temperature dependence of the heat capacity $C(T)$ (upper) and the entropy $S(T)$ (lower) of the dipolar Cairo spin ice with $N = 20$ dipoles at $c = 376$ nm in long-

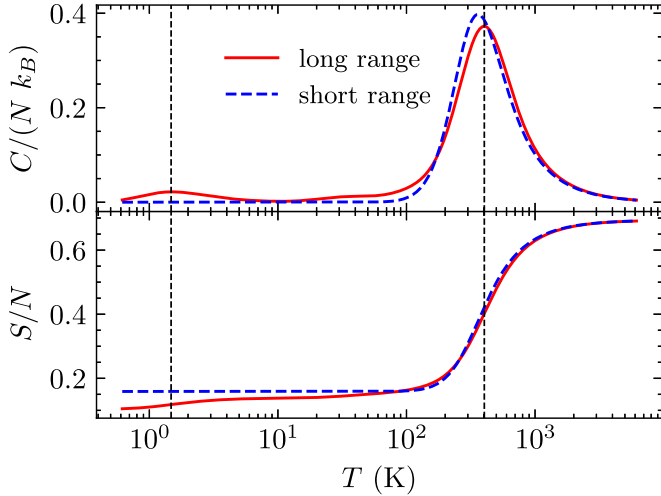


FIG. 3. Temperature dependence of the heat capacity $C(T)$ (upper) and entropy $S(T)$ (lower) of the dipolar Cairo spin ice with $N = 20$ dipoles at $c = 376$ nm in long-range interaction and short-range interaction models. The dashed vertical lines indicate temperatures of heat capacity peaks.

and short-range models with PBCs in Fig. 3. As well as the Monte Carlo method, the exact solution shows the presence of a low-temperature peak in the heat capacity for a model with long-range interactions, and the absence of it in a short range. A high-temperature peak is present in both models.

It can be explained by analyzing the exact solution of the temperature behavior of the entropy. The residual entropy $S(T \rightarrow 0)$ in the two considered models has different values. In a model with a long interaction radius, the degeneracy multiplicity of the GS is smaller, while in a short range it is greater. Thus, there is a pronounced increase in S for a long-range model. The peak temperature of the heat capacity coincides with the temperature of the maximum entropy growth rate. The high-temperature peak of the heat capacity is accompanied by an increase in entropy. But the reasons for the increase in entropy at low and at high temperatures are different.

Figure 4 shows the heights of the heat capacity peaks as a function of the dipole quantity. The height in the high-temperature region does not change at an increase in N , neither in the long-range interaction model [$C(T_2^p)$] nor in the short-range interaction model (C_{peak}). The value of C_{peak} is less than $C(T_2^p)$ since the rate of change in the average energy is proportional to the number of pair energies, which will naturally be larger in the case of a long-range model.

The low-temperature peak in the long-range model grows with increasing N . In Fig. 4 the dashed line indicates the growth function for the low-temperature peak in the long-range model $C(T_1^p) = 0.02476 \ln(N) - 0.0817$, the limit of which is $\lim_{N \rightarrow \infty} C(T_1^p) = \infty$. This confirms the presence of the second-order phase transition. The coefficients of the function are approximated by the method of least squares.

B. Low-energy states and ground state

One of the possible GS configurations for dipolar spin ice on a 2D Cairo lattice with PBCs in both short- and long-range

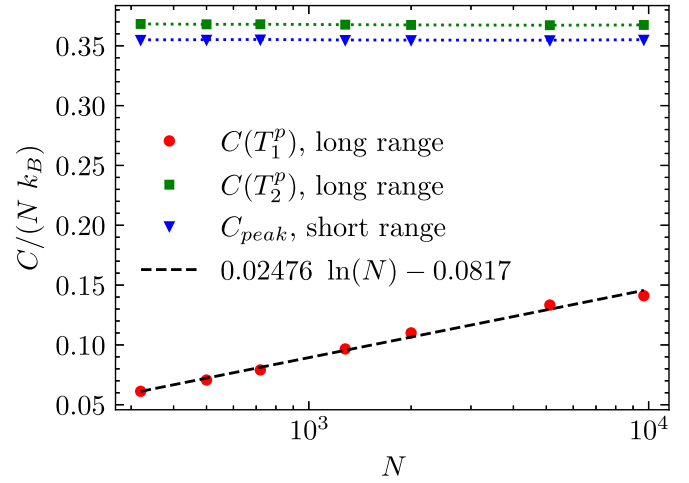


FIG. 4. The value of the heat capacity peak as a function of quantity of dipoles N for the Cairo lattice $c = 376$ nm in both long-range interaction and short-range interaction models.

models is shown in Fig. 1(b). The lattice can be conventionally divided into three sublattices, which consist of horizontal α , vertical β spins, and crosses γ . In GSs of both models, all crosses γ obey the ice rule and have a minimum of energy. The color in Fig. 1(b) indicates the total interaction energy between the α or β types of dipoles and their neighboring four dipoles within the ϵ . Hereafter we will call it the “neighbor energy.”

If we take the energy of one pair of dipoles α and δ as a unit u , then the sum of energies between any of α or β spin and its four neighbors will be one of five possible values: $-4u, -2u, 0, 2u, 4u$. For example, in Fig. 1(b), all α spins have neighbor energy $-4u$, and β 's neighbor energy is 0. Each pair interaction between spins of type β and its neighbors has a mirror pair with the same interaction energy but opposite sign. In the long-range model, spins β also have zero total energy with all interacting spins. The one exception is the long-range interaction between two spins of type β , which makes a small (because of the long distance) negative contribution to the total energy. In the case of open boundary conditions, this pattern will be violated, because not all pairs with β spins will be compensated at the boundaries. For this reason, the configuration of the β sublattice in GSs differs from that presented in [33].

By using the complete enumeration method over all possible states, we have collected all GSs for the system with $N = 20$ and PBCs in long-range and short-range models; see Fig. 5. There are 24 GSs in the short-range model, and eight of those are in the long-range model. Each configuration has a mirrored one with the same energy where all spins are flipped, which is why we consider only the half of states in Fig. 5. In all GSs, dipoles in γ satisfy the ice rule (two in, two out) and have the minimum dipole-dipole interaction energy. That is, dipoles that are on the same line inside the cross always look in the opposite direction.

Spins of the α sublattice are blue (silver), and β spins are red (dim gray) in Fig. 5. Spins with neighbor energy $-2u$ are green (light gray). In row 1 we show the GS for both short- and long-range models. Neighbor energy is 0 for spins of β

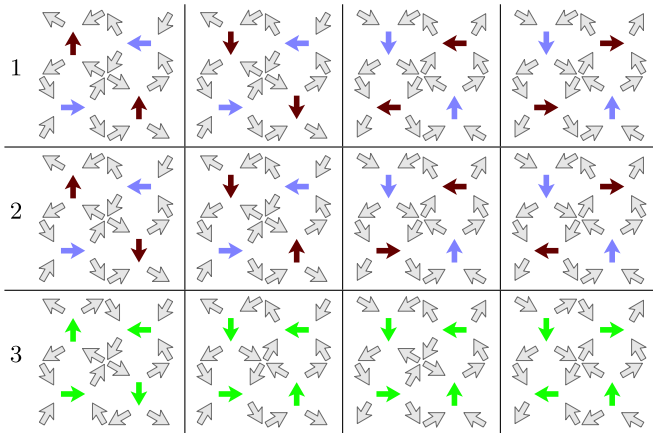


FIG. 5. Ground-state configurations for the dipolar spin ice on the Cairo lattice $L = 2$ with periodical boundary conditions in long-range (row 1) and short-range (rows 1–3) models. We illustrate only half of the configurations, implying that the other half is similar but with all spins inverted.

sublattice. Only long-range interactions between them affect ordering, and energy is minimized between codirected spins. That is why β spins have ferromagnetic order. Configurations of row 2 are equal to row 1, but β spins have chaotic order. The energy of these configurations is the same in the short range, but slightly higher in the long range because of the positive energies between the β spins. So configurations of row 2 will be GS only for the short range. In row 2 of Fig. 5 every configuration has two β spins which are in antiferromagnetic ordering. The order is not chaotic only because of the small size of the system. The two spins can be either co-oriented or opposite.

The configurations of row 3 are GS only in the short-range model. If we take any configuration from row 2 and turn all spins in any cross γ , all vertical and horizontal spins around the cross will have three pairwise interactions with energy $-u$ and one with energy $+u$. The total energy will remain minimal. In the $N = 20$ lattice with PBCs, all vertical or horizontal spins are adjacent to all the crosses. So we can flip only any one cross. But for a larger lattice we can apply γ rotation locally to the part of the system. All vertical and horizontal spins surrounding the cross must be ordered antiferromagnetically.

The number of configurations in rows 2 and 3 of Fig. 5 grows with increasing N , while row 1 always consists of four configurations (plus four mirrored). The curve $S(T)/N$ experiences a jump in the low-temperature area in the long-range model in Fig. 3. The temperature of the jump corresponds to the temperature of the peak of the heat capacity. The residual entropy has a constant value, and the entropy per spin will tend to be zero at $N \rightarrow \infty$ in the long range. At higher temperatures, the value of $S(T)$ depends on N . The sharpness of the jump of $S(T)/N$ will increase as N increases. This explains the correlation between $C(T_1^p)$ and N for the long-range model in Fig. 4.

In the short-range model, all configurations described in Fig. 5 are GS, so the residual entropy grows with N , and we

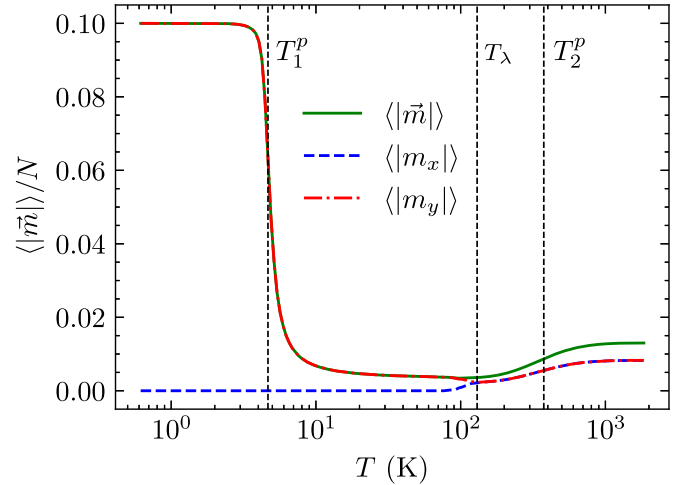


FIG. 6. Temperature behavior of the thermodynamic averaged magnetization of the long-range dipolar spin ice on the Cairo lattice with $N = 5120$ spins and $c = 376$ nm. The green solid line $\langle |\vec{m}| \rangle$ is the total magnetization. The blue dashed line $\langle |m_x| \rangle$ and the red dash-dotted line $\langle |m_y| \rangle$ are the projections of magnetization on the X and Y axes for the same system, respectively.

do not observe changes in entropy and heat capacity in the low-temperature area.

IV. SPIN-SPIN CORRELATIONS

Here we consider only one subset of GSs for the long-range model, where α spins are horizontal and β are vertical. Another case is when the roles of α and β spins are swapped because of the symmetry. This is determined during the freezing of the system. The energy barrier for the the changing roles of α and β is overcome only above the Curie temperature for this system. Both cases of ordering are identical and have the same thermodynamic properties, so we will not consider the second one.

We use the canonical single-spin Metropolis method. It has a known problem of critical slowdown [34]. In our system it holds in the temperature area from $T = 61$ K to $T = 185$ K. We resolved it by running Metropolis from different random high-energy configurations and by averaging the heat capacity values between runs in a given temperature area. Other temperatures were calculated with a single run starting from the GS described above.

Figure 6 shows the temperature behavior of $|\vec{m}|$ and modules of its components $|m_x|$ and $|m_y|$. These parameters are calculated as

$$\begin{aligned}
 |\vec{m}| &= \left| \sum_j^N \vec{m}_j \right| / N, \\
 |m_x| &= \left| \sum_j^N m_{x,j} \right| / N, \\
 |m_y| &= \left| \sum_j^N m_{y,j} \right| / N.
 \end{aligned} \tag{6}$$

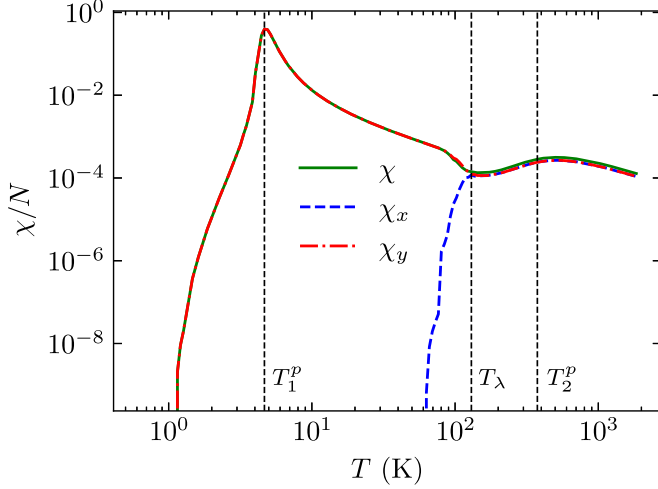


FIG. 7. Temperature behavior of total χ , longitudinal χ_x , and transverse χ_y magnetic susceptibility of the long-range dipolar spin ice on the Cairo lattice with $N = 5120$ spins and $c = 376$ nm.

The γ sublattice satisfies the ice rule in GSs and has a periodic structure of magnetic ordering. The α sublattice has an antiferromagnetic order in GSs. Therefore, $|\vec{m}| = 0$ for the sublattices of α and γ spins in GSs. It can be seen from Fig. 6 that $|m_y| = 0.1$ at $T \rightarrow 0$ because the β sublattice has a ferromagnetic order and consists of $N/10$ spins. The transition of the β sublattice from ferromagnetic to paramagnetic state occurs at temperature T_1^p .

Figure 6 shows that the curves $|m_y|$ and $|\vec{m}|$ are the same at $T < T_\lambda$. This indicates that only β -type spins are remagnetized. The curve $|m_x| = 0$ and does not change at $T < T_\lambda$.

By analogy, we obtained longitudinal and transverse magnetic susceptibility curves (Fig. 7). Susceptibility is calculated as

$$\chi(T) = \frac{\langle |\vec{m}|^2 \rangle - \langle |\vec{m}| \rangle^2}{k_B T N},$$

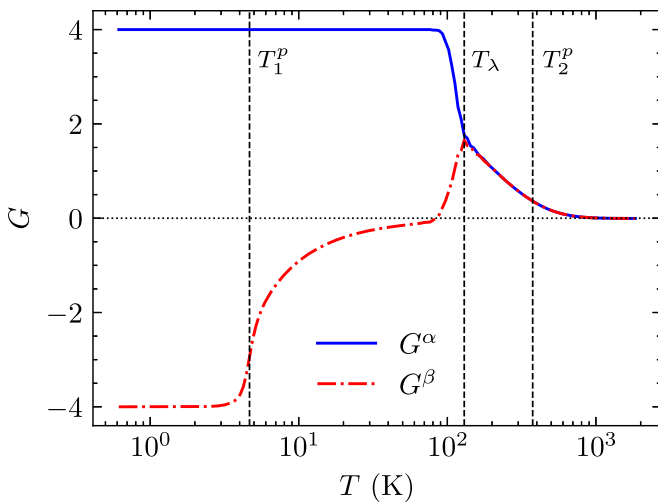


FIG. 8. Temperature behavior of the correlation function for the horizontal G^α and vertical G^β spins of the long-range dipolar spin ice on the Cairo lattice with $N = 5120$ spins and $c = 376$ nm.

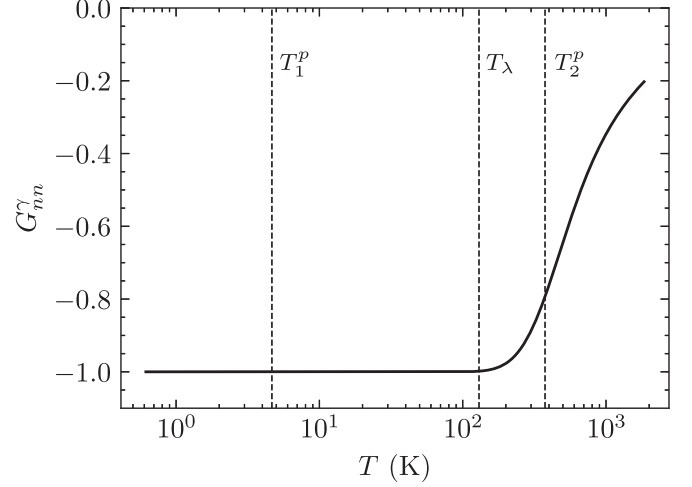


FIG. 9. The correlation function for the nearest neighboring spins of the crosses sublattice γ of the long-range dipolar spin ice on the Cairo lattice with $N = 5120$ spins and $c = 376$ nm.

$$\chi_x(T) = \frac{\langle m_x^2 \rangle - \langle |m_x| \rangle^2}{k_B T N},$$

$$\chi_y(T) = \frac{\langle m_y^2 \rangle - \langle |m_y| \rangle^2}{k_B T N}. \quad (7)$$

The brackets $\langle \rangle$ denote Gibbs thermodynamic averaging. The curves in Fig. 7 show that only vertical spins experience fluctuations at $T < T_\lambda$.

Also, we show the temperature behavior of correlations between the spins of the lattice in Figs. 8, 9 and 11. We define the correlation parameter as

$$G = \sum_i^n \sum_j^m \frac{E_{i,j}}{|E_{i,j}|} / n, \quad (8)$$

where the summation \sum_j^m goes over spins distanced from i spin by a given radius. The sum \sum_i^n includes only the spins that need to be considered in the specific case. The radius

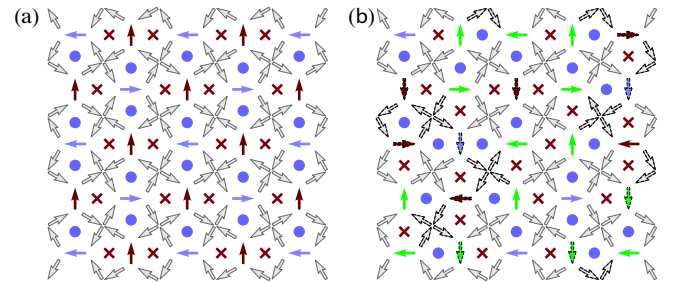


FIG. 10. A part of the dipolar spin ice on the Cairo lattice with $c = 376$ nm. (a) One of the GSs of the long-range model. (b) One of configurations for T_λ . The vertical and horizontal spins have the following color scheme: blue (silver) $E = -4u$, green (light gray) $E = -2u$, and red (dim gray) $E = 0$. The blue circle indicates a pentagon with $E = -5v$, and a red cross is $E = -1v$. The dotted outlines around arrows show the spins that differ from the GS configuration (a).

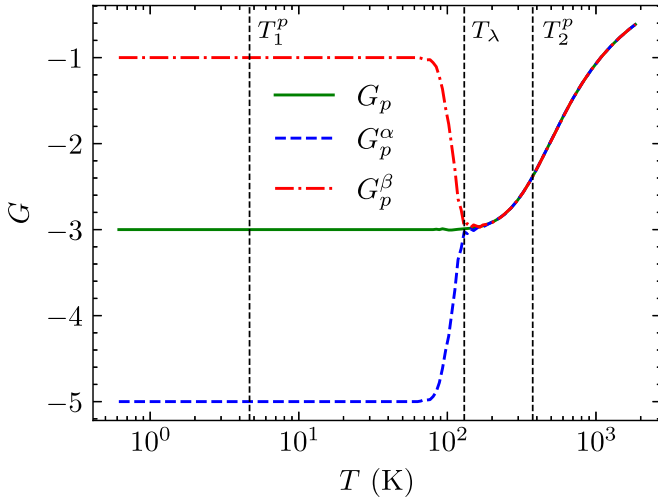


FIG. 11. Temperature behavior of the correlation functions for dipole Cairo spin ice at $c = 376$ nm and $N = 5120$ in the long-range model. G_p is the correlations of spins in all pentagons of the lattice; G_p^α is the correlations of spins in pentagons that contain a horizontal spin from the α sublattice; G_p^β is the correlations of spins in pentagons that contain a vertical spin from the β sublattice.

and the principle of spin selection according to which the correlations are calculated will be defined for each parameter separately.

The correlation parameters G^α and G^β in Fig. 8 take into account only the spins from the α and β sublattices, respectively. The distance between neighboring spins of the α and β sublattice is approximately 1153 nm when the lattice parameter $c = 376$ nm. The α sublattice is ordered antiferromagnetically, and $G^\alpha = 4$ at $T < T_\lambda$. Higher temperature destroys this order, which leads to the disappearance of interspin correlations in the sublattice α . The G^β parameter increases abruptly near T_1^P ; i.e., there is a transition from an ordered ferromagnetic to a disordered state in the β sublattice.

Thus, the temperature behavior of the heat capacity, magnetization, susceptibility, and correlation parameters G^α , G^β show that the low-temperature heat capacity peak at T_1^P is caused entirely by the long-range dipole-dipole interactions between the spins of the β sublattice. The short-range interactions in the Cairo lattice give a zero contribution to energy, and the rest of the lattice (α and γ sublattices) are in the minimal energy state with respect to their nearest neighbors and do not change its configuration. The transition from ferromagnetic order to paramagnetic disorder of spins of the β sublattice in the Cairo spin ice with the long-range interaction model occurs at a temperature T_1^P .

A. High-temperature peak

Figure 2 shows that the high-temperature peak of the heat capacity at T_2^P appears in both short- and long-range dipole-dipole interactions. The magnetization and susceptibility (Figs. 6 and 7) also have high-temperature peaks, but their temperature is slightly higher than T_2^P . The same behavior was observed in square spin ice [4]. Also, the α and β sublattices almost stop correlating at this temperature (Fig. 8).

In Fig. 9 we show the correlation function G_{nn}^γ , which includes only nearest-neighboring interactions between spins in crosses γ [Fig. 1(b)]. The behavior of the curve shows that the order of the closest pairwise interactions breaks down at temperature T_2^P , which leads to a complete disorder of the system.

B. The crossover

The system has a specific behavior around T_λ . This occurs in Figs. 6 and 7 as a merging of the curves for the two sublattices and as the spontaneous anticorrelation of the vertical spins in Fig. 8.

Let us consider the structural element of the Cairo lattice—the pentagon. Any pentagon of the Cairo lattice includes either one α or β spin. The lattice consists of irregular pentagons, and the interaction energy between the nearest spins inside a pentagon is slightly different due to the varying interspin distance and angles. We equate such pairwise interaction energies and denote the energy as v for the sake of simplicity of explanation. We do not use this simplification in our calculations. The minimal energy of the pentagon, when all spins are aligned one after another, will be $E = -5v$, and with one inverted (opposite) spin $E = -3v + 2v = -v$.

Figure 10(a) shows one of the possible configurations of the GS in the long-range model. The blue circle indicates a pentagon with $E = -5v$, and a red cross is $E = -v$. It can be seen that pentagons with $E = -5v$ contain spins of type α , and pentagons with $E = -v$ consist of spins of type β in the GS.

Figure 10(b) shows an example of the configuration of the system at T_λ in the long-range model. We illustrate only a part of the sublattice, which has a continuation on all sides. The dashed outline marks the spins that differ from the corresponding GS configuration. It can be seen that the crosses flip entirely, overcoming a small energy barrier and changing the final energy of the system insignificantly. The ice rule is always satisfied. This behavior does not lead to a dramatic increase in heat capacity, but it affects other thermodynamic characteristics.

Collective remagnetization of the crosses causes a local change in the roles of spins of type α and β . That is, spins with $E = 0$ appear in the α sublattice, and spins with $E = -4u$ appear in the β sublattice. Additionally, spins with $E = -2u$ appear [green in Fig. 10(b)], which are shared by pentagons $E = -5v$ and $E = -v$. The average number of pentagons of both types in the lattice does not change at $T < T_\lambda$. An increase in temperature above T_λ destroys this order.

In Fig. 11 we show the correlation parameters for the pentagons, where only the signs of the energies of the nearest pair interactions are considered for each pentagon. For clarity, we rescaled this plot to represent G_p as the average energy of the nearest pairwise interactions within the pentagon in the units v described above. The pentagon includes five pairs, so G_p may be in the range from $-5v$ to $5v$. G_p^α is the correlations of the pentagons, which contain a horizontal spin from the α sublattice. G_p^β is for pentagons with β -type spins. $G_p = G_p^\alpha + G_p^\beta$ is the spin correlations in all pentagons of the lattice. Figure 11 shows that some of the pentagons of G_p^α near T_λ lose their

correlations, and in G_p^β correlations appear, while their sum G_p remains unchanged.

Thus, we can say that at T_λ the dipolar Cairo lattice has a crossover from a frozen order by crosses to a disorder where the ice rule still remains.

V. CONCLUSIONS

The dipolar spin ice model on the Cairo lattice presents rich and tunable frustrations. It consists simultaneously of crosses, whose behavior was previously studied in the square spin ice [2], and irregular pentagons. At the same time, the lattice can alternatively be divided into three sublattices of crosses, horizontal, and vertical spins.

The phase space of the long-range model is split by three temperatures: T_1^p , T^λ , and T_2^p . Let's define the phases in ascending order by temperature: the completely ordered phase \rightarrow disorder in the sublattice \rightarrow spin ice in crosses \rightarrow disorder. In the completely ordered phase (lowest T), the γ crosses obey the ice rule; the absolute direction in the lattice is governed by the spins of α and β sublattices. α has the antiferromagnetic order, and the energy of its spins with nearest neighbors is minimized. Spins of β sublattice have a ferromagnetic order due to the long-range interactions but become disordered at T_1^p . The crosses γ still satisfy the ice rule in the phase between T_1^p and T^λ . Their absolute positions in the lattice are held by α spins only partially: a cross can be remagnetized with no energy costs if the four surrounding vertical and horizontal spins have an antiferromagnetic ordering. The couplings between δ and β spins break down at T^λ , causing the crosses to no longer maintain their absolute positions in the lattice and to be remagnetized entirely, still obeying the ice rule. The T_2^p breaks the ice rule in γ , and the system transits to a completely disordered state.

In the short-range model, phase space is similar to the long-range one. But there is not the completely ordered low-temperature phase, since there are no long-range interactions that hold an order in the β sublattice. The phases in short-range are disorder in the sublattice \rightarrow spin ice in crosses \rightarrow disorder.

In order to understand and explain the dependence of the heat capacity peak on N from Fig. 4, we need to refer to the definition of the average thermodynamic value of the internal energy at a given T :

$$\langle E \rangle(T) = \frac{\sum_i g(E_i) E_i \exp\left(-\frac{E_i}{k_B T}\right)}{\sum_i g(E_i) \exp\left(-\frac{E_i}{k_B T}\right)}, \quad (9)$$

where the summation goes over all possible values of energy of system and $g(E_i)$ is the quantity of configurations with E_i . This is the definition of the mean value of energy by the Gibbs distribution. The formula (3) comes from the definition of heat capacity $C(T) = \partial \langle E \rangle(T) / \partial T / N$. In other words, the thermal energy at the phase transition is spent to break bonds between spins, the internal energy of which is proportional to the temperature of the phase transition [see the exponent in Eq. (9)]. The height of the heat capacity peak

depends on the number of bonds between spins to be broken at a given temperature. In terms of statistics, the numerator of the heat capacity definition from formula (3) is the variance of the energy in the Gibbs distribution, or a measure of the energy dispersion around its mean value at a given temperature. As shown in [4], the long-range interactions reduce the discretization of the energy space of the system and increase the number of members of the sum in formula (9). The neighboring energy levels are not much different because of the low energy of the pairwise interaction between spins of the β sublattice. The scatter of energies increases the variance in the numerator of formula (3) at T_1^p , which is reciprocal to T^2 , making the heat capacity infinite at $N \rightarrow \infty$ at low temperatures.

In addition, we publish the densities of states and the temperature behavior of the mean energy for the dipolar spin ice on the Cairo lattice $N = 20$ in a comparison of long- and short-range models in the Supplemental Material [35].

The energy of the short-range pair is higher than the long-range one because of the smaller r in the denominator of formula (1). Therefore, short-range interactions are destroyed at higher temperatures. The destruction occurs in two stages: the disappearance of correlations between crosses at T_λ and the destruction of the order inside the crosses at T_2^p . Since the short-range order breaks down in the temperature area instead of a specific temperature, the energy needed to destroy the order is consumed smoothly as the temperature rises. Therefore, there is no infinite peak of the heat capacity at $N \rightarrow \infty$. This effect is called crossover [36,37]. The behavior of $C(T_1^p)$ and C_{peak} in Fig. 4 confirms this fact. The particular temperatures we use to describe the phase transition are defined as the local maximum of the function $C(T)$. The definition is taken from the canonical theory of phase transitions and shows only the local maximum of the function. In fact, phase transition happens in a temperature area, the boundaries of which can be defined only speculatively. By fine tuning the parameters a, b, c it is possible to shift temperatures of transitions separately.

In this paper, using calculations with the canonical Metropolis algorithm, we have shown that the two-dimensional Cairo lattice can have a long-range order in our model. Long-range interactions at approximately 1153 nm distance with the lattice parameter $c = 376$ nm show a low-temperature order-disorder phase transition in the β sublattice spins, which are frustrated when considering the short-range model.

A lattice with similar geometry, parameters a, b, c , and M , was considered earlier in [23]. In the experiment, the authors cooled the system below the so-called blocking temperature 130 K, which ensures that configurations remain frozen during x-ray magnetic circular dichroism imaging after thermal annealing. This temperature coincides with our T_λ , which is not the GS but meaningful in our results. The reason that system blocks at 130 K in the experiment [23] may be in the relaxation time of macrospins, which increases dramatically at low temperatures, and may be longer than the time of the experiment. The second reason is the annealing procedure. The system may be stuck at a local energy minimum while cooling down. Based on our results on the GS structure, it is possible to control the reachability of the GS during the

cooling of spin ice in the experiment. Estimated relaxation times are a good subject for further research. The third reason could be local defects or imprecisions in the geometry of the experimental sample. Long-range interactions have an effect only if all short-range pairwise interactions for the spins of the β sublattice are fully compensated.

Despite the low-temperature T_1^P for the lattice geometry taken as the basis, it would be interesting to experimentally verify the existence of a low-temperature heat capacity peak and a magnetic susceptibility. The increase in temperature T_1^P could be achieved by increasing the M_s of the material.

ACKNOWLEDGMENTS

We thank Alan Farhan for valuable discussions. This work was done on the IAM FEB RAS supercomputer cluster. Research with the canonical single-spin Metropolis algorithm was financially supported by the state task of the Ministry of Science and Higher Education of the Russian Federation No. 122052500009-6, and the investigation with the complete enumeration method was performed in the frame of a grant of the President of the Russian Federation for state support of the leading scientific schools No. NSh-2559.2022.1.2.

-
- [1] Y. Shevchenko, K. Nefedev, and Y. Okabe, *Phys. Rev. E* **95**, 052132 (2017).
- [2] R. Wang, C. Nisoli, R. Freitas, J. Li, W. McConville, B. Cooley, M. Lund, N. Samarth, C. Leighton, V. Crespi *et al.*, *Nature (London)* **439**, 303 (2006).
- [3] C. Nisoli, R. Moessner, and P. Schiffer, *Rev. Mod. Phys.* **85**, 1473 (2013).
- [4] Y. Shevchenko, A. Makarov, and K. Nefedev, *Phys. Lett. A* **381**, 428 (2017).
- [5] M. J. Morrison, T. R. Nelson, and C. Nisoli, *New J. Phys.* **15**, 045009 (2013).
- [6] S. H. Skjærø, C. H. Marrows, R. L. Stamps, and L. J. Heyderman, *Nat. Rev. Phys.* **2**, 13 (2020).
- [7] J. Park, B. L. Le, J. Sklenar, G.-W. Chern, J. D. Watts, and P. Schiffer, *Phys. Rev. B* **96**, 024436 (2017).
- [8] Y. Li, T. Wang, Z. Hou, H. Liu, X. Dai, and G. Liu, *Phys. Lett. A* **380**, 2013 (2016).
- [9] G.-W. Chern, M. J. Morrison, and C. Nisoli, *Phys. Rev. Lett.* **111**, 177201 (2013).
- [10] I. Gilbert, G.-W. Chern, S. Zhang, L. O'Brien, B. Fore, C. Nisoli, and P. Schiffer, *Nat. Phys.* **10**, 670 (2014).
- [11] I. Gilbert, Y. Lao, I. Carrasquillo, L. O'Brien, J. D. Watts, M. Manno, C. Leighton, A. Scholl, C. Nisoli, and P. Schiffer, *Nat. Phys.* **12**, 162 (2016).
- [12] X. Zhang, A. Duzgun, Y. Lao, S. Subzwari, N. S. Bingham, J. Sklenar, H. Saglam, J. Ramberger, J. T. Batley, J. D. Watts *et al.*, *Nat. Commun.* **12**, 6514 (2021).
- [13] H. Stopfel, U. B. Arnalds, A. Stein, T. P. A. Hase, B. Hjörvarsson, and V. Kapaklis, *Phys. Rev. Mater.* **5**, 114410 (2021).
- [14] G.-W. Chern, P. Mellado, and O. Tchernyshyov, *Phys. Rev. Lett.* **106**, 207202 (2011).
- [15] G.-W. Chern and O. Tchernyshyov, *Philos. Trans. R. Soc. A* **370**, 5718 (2012).
- [16] G. Möller and R. Moessner, *Phys. Rev. B* **80**, 140409(R) (2009).
- [17] A. G. Makarov, K. Makarova, Y. A. Shevchenko, P. D. Andriushchenko, V. Y. Kapitan, K. S. Soldatov, A. V. Perzhu, A. Rybin, D. Y. Kapitan, E. Vasilev *et al.*, *JETP Lett.* **110**, 702 (2019).
- [18] U. B. Arnalds, A. Farhan, R. V. Chopdekar, V. Kapaklis, A. Balan, E. T. Papaioannou, M. Ahlberg, F. Nolting, L. J. Heyderman, and B. Hjörvarsson, *Appl. Phys. Lett.* **101**, 112404 (2012).
- [19] I. Rousochatzakis, A. M. Läuchli, and R. Moessner, *Phys. Rev. B* **85**, 104415 (2012).
- [20] A. M. Abakumov, D. Batuk, A. A. Tsirlin, C. Prescher, L. Dubrovinsky, D. V. Sheptyakov, W. Schnelle, J. Hadermann, and G. Van Tendeloo, *Phys. Rev. B* **87**, 024423 (2013).
- [21] M. Rojas, O. Rojas, and S. M. de Souza, *Phys. Rev. E* **86**, 051116 (2012).
- [22] A. A. Tsirlin, I. Rousochatzakis, D. Filimonov, D. Batuk, M. Frontzek, and A. M. Abakumov, *Phys. Rev. B* **96**, 094420 (2017).
- [23] M. Saccone, K. Hofhuis, Y.-L. Huang, S. Dhuey, Z. Chen, A. Scholl, R. V. Chopdekar, S. van Dijken, and A. Farhan, *Phys. Rev. Mater.* **3**, 104402 (2019).
- [24] C. Castelnovo, R. Moessner, and S. L. Sondhi, *Nature (London)* **451**, 42 (2008).
- [25] Y. A. Shevchenko, A. Makarov, P. Andriushchenko, and K. Nefedev, *J. Exp. Theor. Phys.* **124**, 982 (2017).
- [26] R. G. Melko, B. C. den Hertog, and M. J. P. Gingras, *Phys. Rev. Lett.* **87**, 067203 (2001).
- [27] R. G. Melko and M. J. P. Gingras, *J. Phys.: Condens. Matter* **16**, R1277 (2004).
- [28] A. Farhan, P. Derlet, A. Kleibert, A. Balan, R. Chopdekar, M. Wyss, L. Anghinolfi, F. Nolting, and L. J. Heyderman, *Nat. Phys.* **9**, 375 (2013).
- [29] A. Farhan, P. M. Derlet, A. Kleibert, A. Balan, R. V. Chopdekar, M. Wyss, J. Perron, A. Scholl, F. Nolting, and L. J. Heyderman, *Phys. Rev. Lett.* **111**, 057204 (2013).
- [30] L. Anghinolfi, H. Luetkens, J. Perron, M. Flokstra, O. Sendetskyi, A. Suter, T. Prokscha, P. Derlet, S. Lee, and L. Heyderman, *Nat. Commun.* **6**, 8278 (2015).
- [31] N. Metropolis, A. W. Rosenbluth, M. N. Rosenbluth, A. H. Teller, and E. Teller, *J. Chem. Phys.* **21**, 1087 (1953).
- [32] W. K. Hastings, *Biometrika* **57**, 97 (1970).
- [33] K. Makarova, V. Strongin, I. Titovets, A. Syrov, I. Zinchenko, V. Samoylov, K. Hofhuis, M. Saccone, A. Makarov, A. Farhan *et al.*, *Phys. Rev. E* **103**, 042129 (2021).
- [34] H. Gould and J. Tobochnik, *Comput. Phys.* **3**, 82 (1989).
- [35] See Supplemental Material at <http://link.aps.org/supplemental/10.1103/PhysRevE.106.064105> for the exact densities of states and the temperature behavior of the mean energy for the dipolar spin ice on the Cairo lattice with 20 spins.
- [36] S. Gluzman and V. I. Yukalov, *Phys. Rev. E* **58**, 4197 (1998).
- [37] H. Nishimori and G. Ortiz, in *Elements of Phase Transitions and Critical Phenomena* (Oxford University Press, Oxford, 2010), p. 79.